Core/Shell CdSe/CdTe Heterostructure Nanowires Under Axial Strain

T. Sadowski and R. Ramprasad*

Chemical, Materials, and Biomolecular Engineering, Institute of Materials Science, University of Connecticut, Storrs, Connecticut 06269

Received: July 27, 2009; Revised Manuscript Received: October 20, 2009

An ab initio computational study was performed to assess the impact of uniaxial strain (along the wurtzite *c* axis) on the electronic structure of CdSe and CdTe systems of decreasing dimensionality. In bulk situations, the band gap of CdSe under tension behaves as expected, decreasing with increasing *c*, whereas CdTe under compression is accompanied by an sp^3 to sp^2 transition that results in a decrease in the band gap. Through a series of two-dimensional heterostructure slabs, the impact of strain on the valence band offset (VBO) between CdSe and CdTe was considered and found to decrease with increasing *c* lattice parameter. The variation of the band gap of single-component CdSe and CdTe nanowires strictly follows the trends obtained in the bulk calculations, although the absolute values of the nanowire band gap were larger due to quantum confinement. The impact of strain on the VBO in core/shell heterostructure nanowires was found to depend on the choice of core material. When CdSe is used as the core material, the VBO increases with increasing *c* lattice parameter, whereas when CdTe is used as the core material, the VBO decreases with increasing *c*. Regardless of the choice of core material, the overlap between the electron and hole states was found to be quite low in these structures and depends only weakly on strain.

I. Introduction

One of the challenges that severely restricts the widespread usage of current thin-film-based photovoltaic devices is their low solar-to-electrical conversion efficiency.[1] A major factor that limits this conversion efficiency is the rapid relaxation of high-energy photoexcited excitons to lower energies, resulting in the conversion of their excess energy to heat through phonon emission.[2,3] The second factor that impacts the efficiency is the dissociation of photoinduced excitons into free electrons and holes, rather than their recombination. In current thin-film Si-based photovoltaic devices, this latter step is accomplished through the built-in electric fields at p−n junctions.

Recent theoretical and experimental studies[4–7] indicate that quantum confinement and the associated discrete energy levels in semiconductor nanocrystals (NCs) result in a slowed rate of exciton decay[8] and the generation of multiple excitons rather than phonons at photon energies larger than the band gap.[9] Exciton dissociation in such NC-based architectures may be enabled by suitable interfaces between dissimilar materials, for example, those displaying a Type II band offset in which the valence and conduction band edges on either side of the interface are staggered,[10–13] as shown schematically in Figure 1. Among heterojunction NCs, core/shell nanorods and nanowires offer a further advantage. In addition to the possibility of efficient creation and dissociation of excitons, they provide separate channels for the transport of the dissociated charge carriers. Exploiting modern colloidal chemistry techniques, it is currently possible to fabricate heterojunction NCs with atomic level control over their geometry[14] and the composition across the interface,[15] thereby opening up new pathways for the design of NC-based, high efficiency, photovoltaic devices.[16–20]

Here, we focus on the electronic structure of core/shell (0001) CdSe/CdTe nanowires under strain, with CdSe and CdTe being in the wurtzite phase and coherent across the core/shell interface (Figure 1). The axis of the nanowire is chosen to be along the (0001) axis, as this is the preferred growth direction for wurtzite nanowires.[22] CdSe and CdTe are two of the most frequently studied members of the chalcogenide family as their band gaps fall within the visible spectrum, making them extremely attractive for photovoltaic applications.[21] Nevertheless, due to significant lattice mismatch (≈7%) between the two systems, coherent core/shell systems are expected to be under uniaxial strain, and this can significantly affect the band gaps and band offsets across the interface. Owing to their large surface area-to-volume ratio, heterostructure nanowires have been found to allow for large lattice mismatches without the formation of extended defects at the interface.[23–27] Although the band offset between CdSe and CdTe has been studied before in the context of bulk heterojunctions,[28,29] the band offset in nanowires is expected to differ due to the uniaxial strain as well as quantum confinement effects. At present, such information is lacking and

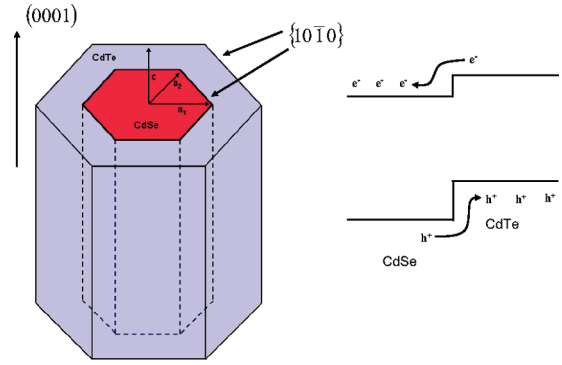

Figure 1. Schematic diagram of the core/shell CdSe/CdTe nanowires considered in this study (left) and the expected Type II band offset across the CdSe/CdTe interface (right), illustrating a possible mechanism of electron−hole separation. The wire is oriented along the wurtzite (0001) direction with nonpolar {10$\bar{1}$0} interfaces and surface facets.

* To whom correspondence should be addressed. E-mail: rampi@ims.uconn.edu.

10.1021/jp907150d
Published on Web 01/07/2010

a fundamental study of the role of anisotropic strain on the electronic properties of wurtzite CdSe and CdTe would prove useful as a roadmap for predictive heterostructure design.

In this ab initio computational study, we present a critical analysis of the impact of uniaxial strain (along the wurtzite *c* axis) on the electronic structure of CdSe and CdTe systems. Although core/shell nanowires constitute our primary interest, we consider systems with progressively decreasing dimensionality, starting with bulk CdSe and CdTe, followed by CdSe/CdTe slab heterostructures, and finally, CdSe, CdTe, and CdSe/CdTe core/shell nanowire geometries.

After providing details of our calculations in section II, we begin with a discussion of our bulk CdSe and CdTe results in section III.A. Under uniaxial strain along the *c* axis, we find that the band gap of CdSe behaves as expected in an sp^3-bonded covalent system, decreasing with increasing *c*. On the other hand, CdTe displays an unusual behavior—its band gap initially increases upon compression but goes through a maximum and decreases upon further compression. We find that this "anomalous" behavior is accompanied by a transition from sp^3 to sp^2 hybridization upon compression. Next, in section III.B, we consider the impact of strain on the valence band offset (VBO) between CdSe and CdTe through a series of two-dimensional heterostructure slabs. Using the valence band edge in the bulklike region sufficiently far from the interface to define the VBO, we find that it decreases with increasing *c* lattice parameter. Finally, we consider nanowires in section III.C. The behavior of single-component CdSe and CdTe nanowires (section III.C.1) when subject to uniaxial strain is consistent with bulk calculations. A series of core/shell heterostructure nanowires of varying core and shell thickness were then considered (section III.C.2). When CdSe is used as the core material, the VBO increases with increasing *c* lattice parameter, whereas when CdTe is used as the core material, the VBO decreases with increasing *c*. In an attempt to quantify the tendency for exciton dissociation, we have also performed an analysis of the overlap of the highest occupied (hole) and lowest unoccupied (electron) states (section III.C.3) in single-component and core/shell nanowires. We find that, in single-component nanowires, there is significant overlap between the electron and hole states, whereas in the core/shell nanowires, the overlap is significantly low (implying low and high probability of exciton dissociation, respectively). Uniaxial strain along the nanowire axis does not change the overlap appreciably. We conclude the paper with a summary in section IV.

II. Methods

All calculations for this study are based on the Kohn−Sham density functional formalism,[30] as implemented within SIESTA,[31] a local orbital density functional theory (DFT) code. The exchange-correlation effects are treated using the local density approximation (LDA) as parametrized by Perdew and Zunger.[32] The deficiencies of LDA are well-known, especially in the II−VI family of semiconductors, where the band gap may be underestimated by as much as 50%.[33] On the basis of our prior work[34,35] as well as the work of others,[36] we argue that *changes* in band-gap values trend well across the strains considered in this study. Moreover, we stress that the valence band states used to derive the VBO are ground-state properties and thus well-represented by DFT.[37]

Core electrons were described by norm-conserving pseudopotentials, constructed according to the Troullier−Martins scheme.[38] The valence state configurations for Cd, Se, and Te are $[Kr]5s^24d^{10}$, $[Ar3d^{10}]4s^24p^4$, and $[Kr4d^{10}]5s^25p^4$, respectively.

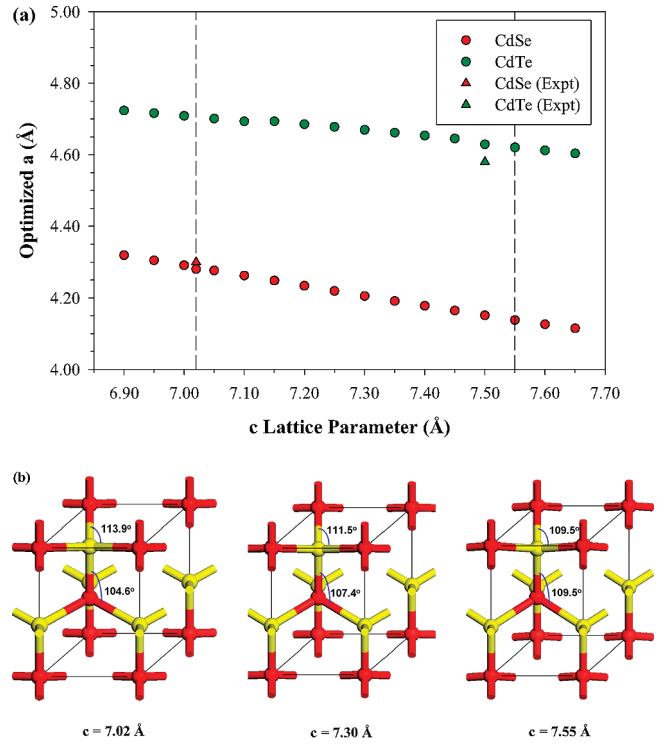

Figure 2. (a) Optimal *a* lattice parameter as a function of the fixed *c* lattice parameter. Vertical dashed lines indicate the equilibrium values of CdSe and CdTe. The corresponding experimental values are shown for comparison. (b) Structural changes in wurtzite CdTe as a function of the *c* lattice parameter.

The additional computational cost associated with including semicore states of Cd, Se, and Te in the valency was not required, as it was not found to significantly improve results. The valence electron wave functions were expanded using a double-ζ plus polarization (DZP) basis set with an orbital confining cutoff radius specified by an energy shift parameter of 0.002 Ry. Sampling the Brillouin zone of bulk CdSe and CdTe using a (6 × 6 × 6) Monkhorst−Pack[39] *k*-point mesh yielded well-converged results. From these calculations, it was determined that the equilibrium *a* and *c* lattice constants for CdSe were 4.29 and 7.02 Å and those for CdTe were 4.62 and 7.55 Å, in good agreement with prior work at the same level of theory[40] and with the corresponding experimental values.[41,42] For the slab and nanowire calculations, a (6 × 1 × 6) and a (1 × 1 × 10) Monkhorst−Pack *k*-point mesh were employed to yield converged results. Relaxation of all structures was accomplished by requiring the forces experienced by each atom to be smaller than 0.04 eV/Å. Where necessary, the underlying local symmetry was broken to ensure relaxation to the ground state.

III. Results

A. Bulk Calculations. When subjected to a uniaxial strain, the atoms in a nanowire have more freedom to expand or contract along the radial direction due to the free surface. To mimic such a strain in a bulk environment, a series of calculations constraining the bulk system at a fixed *c* lattice parameter (but with the *a* lattice parameter optimized) were performed. The value of *c* was chosen to lie between 6.90 and 7.65 Å in increments of 0.05 Å. This range was specifically chosen to include the bulk lattice parameters of CdSe and CdTe. A summary of these results is presented in Figure 2a. For both CdSe and CdTe, a compression (stretching) of the *c* axis

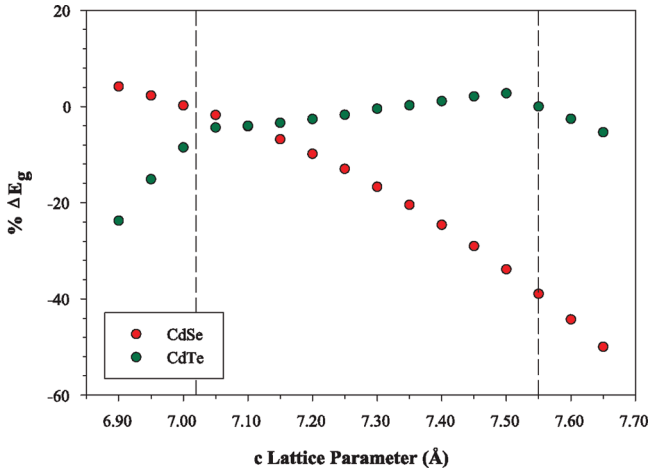

Figure 3. Deviation in bulk band gap from equilibrium CdSe and CdTe LDA values as a function of the *c* lattice parameter. Vertical dashed lines indicate the equilibrium values of CdSe and CdTe.

increases (decreases) *a* from its equilibrium value. For comparison, the calculated equilibrium values of the lattice parameters for wurtzite CdSe and CdTe, along with the corresponding experimental values, are also shown in Figure 2a.

Once the individual optimized *a* lattice parameters were determined for each value of *c*, the band structure of hexagonal CdSe and CdTe was plotted to determine how strain impacts not only the band structure but also the magnitude of the energy gap. Figure 3 presents the percentage change in the band gap from the unstrained, bulk LDA values as a function of the *c* lattice parameter. The experimentally determined band-gap values at equilibrium are approximately 30% larger[41,42] than the LDA equilibrium values of 1.23 and 1.15 eV for CdSe and CdTe, respectively. For CdSe, the observed band-gap behavior with varying *c* lattice parameter can be rationalized using simple molecular orbital theory. As the atoms in the axial direction are compressed (stretched), the electrostatic repulsion between the electrons in the orbitals increases (decreases), widening (narrowing) the gap between the highest occupied bonding and lowest unoccupied antibonding states.

In the case of CdTe, the band gap does not consistently increase with decreasing *c* lattice parameter. At small compressions from equilibrium (up to $c = 7.50$ Å), the band gap of CdTe increases by approximately 3% over the equilibrium LDA value. Below 7.05 Å, the rate of decrease in band gap with *c* changes once again and becomes quite large.

To further understand the origin of the two "turning points" in the case of CdTe at *c* lattice parameter values of 7.50 and 7.05 Å, we focus on the band structure. Figure 4 shows the CdSe and CdTe band structure at three different lattice parameters: the equilibrium *c* lattice parameters of CdSe and CdTe as well as one equidistant between the two. For the range of lattice parameters considered in this study, the valence band maximum (VBM) and conduction band minimum (CBM) remain located at the Γ point. Aside from the LDA error, the CdSe and CdTe plots at equilibrium compare favorably with prior work.[40] To our knowledge, no other experimental or theoretical results exist for either CdTe or CdSe subject to a uniaxial strain. In the case of CdSe, consistent with the band-gap results of Figure 3, we see that the CBM position systematically decreases with respect to the VBM position for progressive increases of the *c* lattice parameter.

Bulk CdTe, on the other hand, displays a more complex behavior (Figure 4b), consistent with the band-gap results of Figure 3. To better understand this behavior, we show a portion of the band structure of CdTe at its equilibrium lattice constant in Figure 4c, with the key bands labeled. At equilibrium, the VBM (V_1) and the CBM (C_1) are dominated by the Te 5p and Cd 5s states, respectively, as expected. Upon uniaxial compression, the relative positions of the V_1 and C_1 bands, as well as the V_2 and C_2 bands, begin to change. Below 7.50 Å, V_2 (composed of Cd 5p states) overtakes V_1 as the VBM and the band gap begins to decrease. At 7.05 Å, C_2 (composed of both Cd and Te 5p states) becomes lower in energy than the previous CBM C_1. Below this level of compression, interesting structural changes occur. As shown in Figure 2b, each Cd (Te) atom is tetrahedrally bonded to four Te (Cd) atoms, as required by sp^3 hybridization at equilibrium. At a high level of compression, the Cd (Te) atoms tend to become coplanar with three of the Te (Cd) atoms, thereby approaching sp^2 hybridization. It is the onset of such structural changes that drives the decrease in the band gap.

These bulk calculations have important implications. Referring to Figure 3, it is apparent that the band gaps of *both* CdSe and CdTe decrease relative to their corresponding equilibrium values, despite the fact that one of them (CdSe) is under tension and the other (CdTe) is under compression. The unanticipated behavior and accompanying structural changes under compression are not limited to CdTe. We have observed similar behavior in CdSe as well as ZnX (X = O, S, Se, Te),[43] which leads us to believe it is universal in II−VI semiconductors. This perhaps explains recent ab initio results[18] dealing with ZnO/ZnS and ZnO/ZnTe core/shell nanowires where the band gaps of the core *and* shell material have been shown to decrease relative to their equilibrium values.

B. Slab Calculations. With a reasonable understanding of the behavior of band gaps of bulk CdSe and CdTe under uniaxial strain, we move on to the impact of such a strain on the VBO of CdSe/CdTe two-dimensional heterostructures. As shown in Figure 1, the heterostructure nanowires to be considered later have interfaces along hexagonal $\{10\bar{1}0\}$ planes. To mimic such an interface in a two-dimensional environment, a CdSe/CdTe heterostructure slab containing a $(10\bar{1}0)$ interface was created, with eight layers each of CdSe and CdTe. The impact of strain was assessed for three choices of the *a* and *c* lattice parameters: (i) at the equilibrium bulk CdSe values, (ii) at the equilibrium bulk CdTe values, and (iii) at the equilibrium values for the chosen slab supercell, obtained through an unconstrained optimization. All of these values are listed in Table 1. To obtain an estimate of the band gap and the VBO for the three different structures, the layer decomposed density of states (LaDOS)[44] was determined. The LaDOS for each layer was obtained by summing the density of states (DOS) projected from each atom in a layer and dividing by the total number of CdX (X = Se, Te) pairs in that layer. In computing the LaDOS, the energy eigenvalues were smeared with Gaussians of a width of $\sigma = 0.100$ eV. To test the accuracy of the LaDOS approach, the band lineup method of Van de Walle and Martin[45] was also used to determine the VBO in the heterostructure. We find that the results from the two approaches are quite similar, differing by ≈0.10 eV.

Figure 5 shows the VBM and CBM within the heterostructure slab as a function of the CdSe or CdTe layer position normal to the interface plane for the three strain conditions considered, labeled according to their *c* value. In the interior of each component of the slab, (enclosed by vertical dashed lines) the band gaps are bulklike and comparable to the values reported in Figure 3 for CdSe and CdTe constrained to lie at an identical

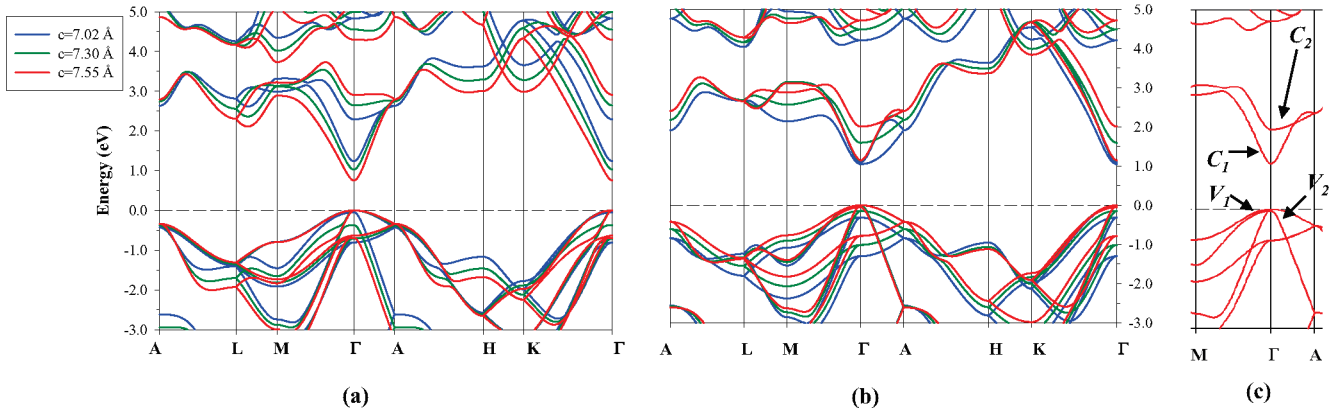

Figure 4. Band structure of wurtzite (a) CdSe and (b) CdTe as a function of the *c* lattice parameter. (c) Band structure of CdTe at its equilibrium lattice constant ($c = 7.65$ Å) in a small range of energies about the Γ point. The labels V_1, V_2, C_1, and C_2 are used to indicate bands that move upon compression. The zero of energy in each was chosen to correspond to the VBM.

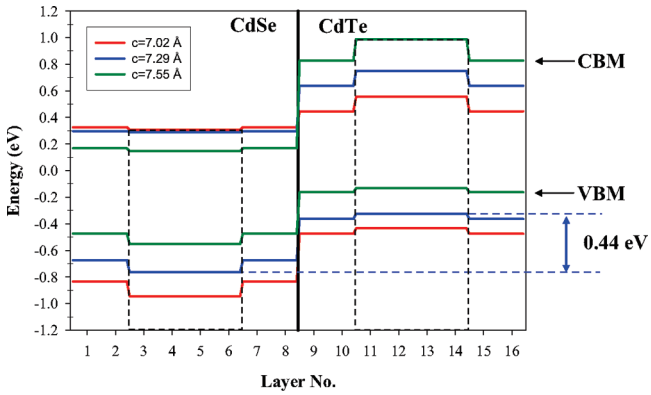

Figure 5. LaDOS for the three different lattice constants considered, labeled according to the axial *c* value. The zero point of energy was chosen to correspond to the Fermi energy. The solid vertical line between layers 8 and 9 represents the interface separating the CdSe layers on the left from the CdTe layers. The VBO indicated on the plot corresponds to the optimal (strain-minimized) structure.

TABLE 1: Lattice Constant *a* (in Å), Band Gap E_g (in eV), and Valence Band Offset VBO (in eV) of the Bulklike Regions of the Heterostructure Slab as Well as E_g for Bulk CdSe and CdTe at Its Optimized *a* Lattice Parameter Corresponding to That *c* Lattice Parameter

		CdSe			CdTe			
c	a_{slab}	a_{bulk}	E_g^{bulk}	E_g^{slab}	a_{bulk}	E_g^{bulk}	E_g^{slab}	VBO
7.02	4.28	4.28	1.23	1.25	4.70	1.05	0.99	0.51
7.27	4.45	4.21	1.07	1.05	4.67	1.14	1.07	0.44
7.55	4.62	4.14	0.75	0.70	4.62	1.15	1.12	0.42

c value. A summary of these results, as well as the corresponding bulk band-gap values, are presented in Table 1.

Beyond the bulklike layers, the presence of an interface results in the reduction of the band gap. On either side of the interface, the band gaps are, in general, comparable but not aligned, creating a VBO between the two materials. Defining the VBO as the difference in the valence band edges between the bulklike CdSe and CdTe layers, we find that the magnitude varies inversely with increasing *c*. At the optimal lattice positions, the VBO is 0.44 eV, less than the value reported in the theoretical studies of Wei and Zunger,[28,29] who found the natural (strain-free) VBO between bulk CdSe and CdTe in their zinc blende phases to be 0.60 eV.

This disparity in values can be attributed to the fact that, for all lattice parameters considered, at least one side of the heterostructure was strained to a position far from the optimal *a* value corresponding to the choice of *c*, which strongly affects the location of the VBM, especially in CdSe. To illustrate this point, consider the VBM in the CdSe bulklike region. At the equilibrium bulk CdSe lattice parameters, the VBM in this region is roughly 0.1 eV below the VBM in the interface layers. As the system is stretched to the equilibrium lattice parameters of CdTe, the difference in energies between the VBM in the bulklike and interface region decreases to roughly half this value. Conversely, in the CdTe bulklike region, the difference between the bulklike and interface VBM remains the same as the system is stretched. The higher sensitivity of CdSe relative to CdTe to strain persists in the nanowire geometries to be discussed next.

C. Nanowire Calculations. Building upon our findings in the bulk and two-dimensional geometries, we now focus upon the impact of uniaxial strain on the band gap and VBO of single-component and core/shell nanowires, respectively. In our previous study of CdSe (0001) nanowires,[35] we reported that nanowires with hexagonal cross sections are more stable than those with triangular cross sections. Moreover, we found that surface atoms possessing only one dangling bond are able to rehybridize (from sp^3 to sp^2), thereby negating the need for surface passivation. For this aspect of the study, we, therefore, consider a series of unpassivated hexagonal nanowires that are approximately 30 Å in diameter. Generation of these cross sections can be understood by considering the structure in Figure 6a, a single-component nanowire. Beginning with a central hexagon (Ring 1) composed of six pairs of CdX (X = Se, Te), the nanowires were generated by adding three additional rings of hexagonal units, each represented as a yellow shaded region, around Ring 1. Surface facets are terminated by nonpolar $\{10\bar{1}0\}$ planes containing atoms with only one dangling bond. All nanowires are assumed to be infinitely long with a periodic length *c*, oriented along the wurtzite (0001) direction.

Replacing all of the Se atoms in Ring 4 of a CdSe nanowire with Te atoms results in a 3/1 CdSe/CdTe core/shell nanowire (Figure 6b). Performing a similar substitution in Ring 3 of the 3/1 cross section generates a 2/2 nanowire (Figure 6c), consisting of two core rings of CdSe and two shell rings of CdTe. When the identities of Se and Te atoms were interchanged, 3/1 and 2/2 CdTe/CdSe core/shell nanowires were also generated.

1. Single-Component Nanowires. Consider, first, the single-component CdSe and CdTe nanowires with equilibrium *c* lattice parameters of 7.02 and 7.55 Å, respectively. The role of strain was investigated by stretching CdSe to the equilibrium *c* lattice parameter of CdTe and compressing CdTe to the equilibrium *c* value of CdSe. Once the atoms had relaxed in the supercell, an

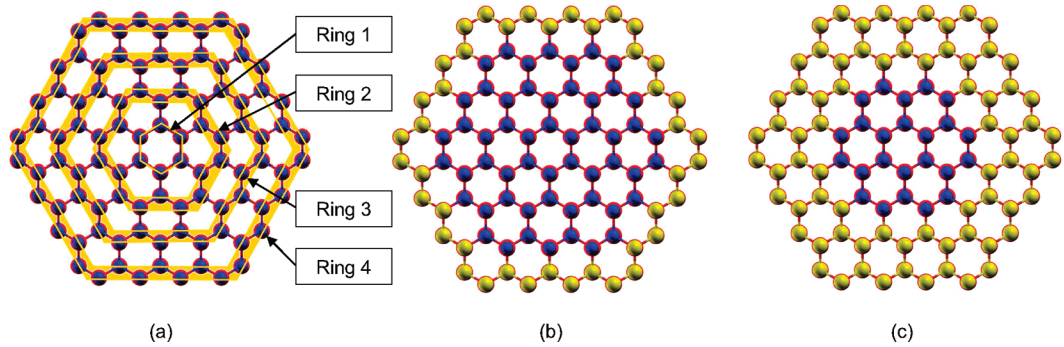

Figure 6. (a) Geometry of the homogeneous CdSe nanowire with Cd and Se represented by red and blue, respectively. The homogeneous CdTe nanowire (not shown) is obtained by replacing all the Se atoms with Te atoms. (b) 3/1 CdSe/CdTe core/shell heterostructure obtained from (a) by replacing the Se atoms in Ring 4 with Te atoms (depicted in gold). (c) 2/2 CdSe/CdTe core/shell heterostructure obtained from (b) by replacing the Se atoms in Ring 3 with Te atoms.

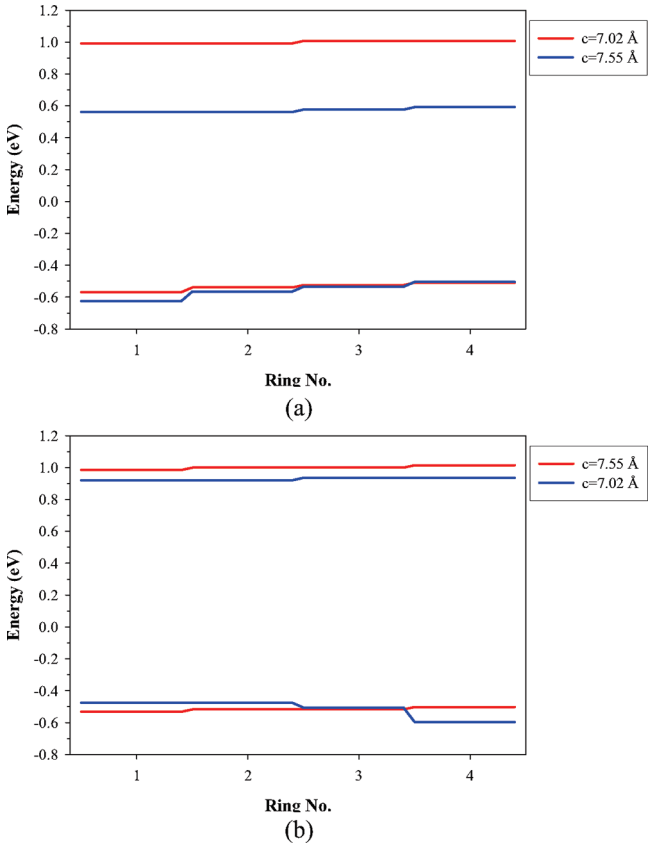

Figure 7. Band gap as a function of ring number for single-component (a) CdSe and (b) CdTe. The red and the blue lines correspond to the valence and conduction band edges of the system lying at its equilibrium and strained c lattice position, respectively. The zero point of energy was chosen to correspond to the Fermi energy.

estimate of the band edges as a function of radial position was determined by an examination of the radially decomposed density of states (RDOS).[35] The RDOS for each ring was obtained by summing the DOS projected from each atom in that ring and dividing by the number of CdX (X = Se, Te) pairs in that ring. The energy eigenvalues for the RDOS were broadened using Gaussians of a similar width to the LaDOS. A summary of the results for both single-component systems are presented in Figure 7.

In both plots, red and blue lines represent the band edges for structures at equilibrium and in a strain state, respectively. When CdSe and CdTe are both lying at their equilibrium coordinates, their band gaps across the innermost ring are ≈0.3 to 0.4 eV higher than their corresponding bulk values (Table 2), reflecting

TABLE 2: Bulk Band Gap (in eV), Band Gap of the Inner Ring (in eV), VBO (in eV), and Electron−Hole Overlap of the Nanowires Considered in This Study. The Dividing Line Is Used to Distinguish the CdSe Core from the CdTe Core Nanowires

System	c	Bulk	E_g^l	VBO	Overlap
CdSe	7.02	1.23	1.56		0.60
	7.55	0.75	1.19		0.55
3/1	7.02	1.23	1.50	0.44	0.20
	7.29	1.03	1.39	0.51	0.19
	7.55	0.75	1.23	0.54	0.15
2/2	7.02	1.23	1.42	0.17	0.14
	7.48	0.82	1.11	0.23	0.12
	7.55	0.75	1.06	0.24	0.11
CdTe	7.02	1.05	1.39		0.58
	7.55	1.15	1.51		0.64
3/1	7.02	1.05	1.22	0.35	0.26
	7.35	1.15	1.35	0.20	0.18
	7.55	1.15	1.39	0.11	0.16
2/2	7.02	1.05	1.14	0.30	0.15
	7.15	1.11	1.16	0.24	0.13
	7.55	1.15	1.22	0.09	0.10

the impact of quantum confinement. It is interesting to note that there is a slight narrowing of the band gap between the core and the surface rings of CdSe. This decrease is small (<0.05 eV) and can be attributed to the increased freedom of movement among the atoms closer to the surface. Consistent with previous studies,[34,35] we find that, as the surface atoms self-passivate, the Cd atoms have a tendency to move inward while the Se atoms move radially outward. Although this behavior is also seen in the CdTe nanowire, the band gap remains constant across all rings.

In the strained nanowires, the band gaps obtained from the innermost rings are significantly smaller than those in the unstrained case, consistent with earlier bulk findings. As with the unstrained CdSe nanowire, the band gap decreases with ring number, albeit to a larger extent. In the CdTe nanowire, axial compression results in noticeable shifts of the CBM and VBM relative to the unstrained system. Unlike the strained CdSe nanowire, the VBM decreases at the surface, resulting in a band gap comparable to that observed in the unstrained CdTe nanowire. This can be attributed to the outward radial movement of the innermost rings when CdTe is under compression. Due to the lack of radial confinement at the surface, the atoms in Ring 4 are able to adopt a more favorable position, causing the increase in band gap.

2. Core/Shell Nanowires. In addition to the single-component systems discussed above, core/shell nanowires with CdSe in

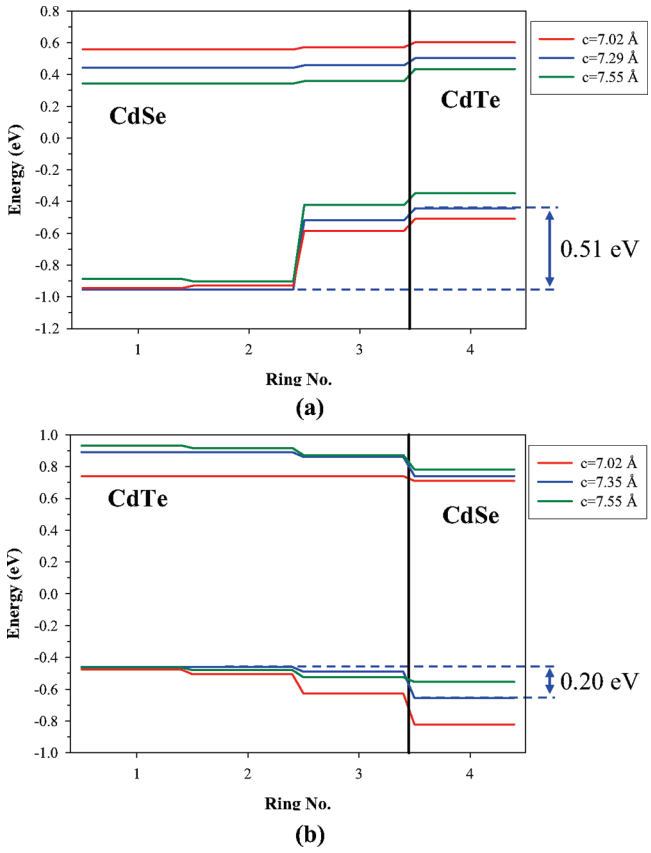

Figure 8. Band gap as a function of ring number for the different lattice constants considered, labeled according to the axial *c* value for the 3/1 (a) CdSe/CdTe and (b) CdTe/CdSe core/shell heterostructures. The zero point of energy was chosen to correspond to the Fermi energy. The solid vertical line indicates the location of the interface separating CdSe from CdTe. The VBO indicated on the plot corresponds to the optimal (strain-minimized) structure and is taken as the difference between the innermost and outermost VBM.

the core and CdTe in the shell (henceforth, referred to as the CdSe core structure), and vice versa (referred to as CdTe core structure), were considered. Furthermore, all geometries are constructed so as to have a coherent interface between the two materials. The relative thicknesses of the core and the shell were varied, resulting in one structure that has a nearly equal ratio of CdSe to CdTe (3/1) and one where there is a much greater concentration of shell material (2/2).

The impact of strain on the electronic properties was assessed by subjecting all systems to axial tension and compression by fixing their coordinates to lie at the *c* lattice parameter of CdTe and CdSe, respectively. An equilibrium lattice parameter, corresponding to a strain-minimized state, was determined for each core/shell structure by performing a series of calculations for different *c* values between 7.00 and 7.60 Å. As with the single-component systems, an estimate of the band gaps and the VBO was determined through an analysis of the RDOS.

Consider first the 3/1 cross sections, whose results are presented in Figure 8a,b for systems with a CdSe and CdTe core, respectively. The optimal *c* lattice parameters in both structures are quite similar, with the CdSe core possessing a value of 7.29 Å and the CdTe core a value of 7.35 Å. Whereas decreasing the lattice parameter increases in the band gap across all rings for the CdSe core heterostructure, the opposite behavior was observed in the CdTe core system. In particular, note the similarity in band-gap values when *c* is at 7.35 and 7.55 Å, a trend that is consistent with prior findings not only for our bulk and single-component nanowire calculations (Table 2) but also the bulklike regions in the two-dimensional heterostructure (Table 1). When the innermost two rings of CdSe and CdTe are compared to the appropriate strained bulk values, there is an increase in the band gap by approximately 0.2 eV due to quantum confinement effects. Moreover, the band gaps across these rings for both the stretched and the compressed states are similar to those in the single-component nanowires at these lattice positions.

Moving out from the innermost two rings toward the interface, a change in the band gap occurs, the magnitude of which varies with the *c* lattice parameter. This change is much more pronounced in the case of the CdSe core where the reduction in the band gap on the CdSe side of the interface results in a large VBO occurring between concentric rings of CdSe and not at the interface. In the case of the CdTe core, there is a slight decrease in the VBM from the innermost values in Ring 3 when at either the optimal or the CdTe lattice parameters. When at the *c* value for CdSe, however, there is a noticeable reduction in the VBM (≈0.13 eV) between Rings 2 and 3. This behavior can be attributed to two factors. The first is the proximity of the interface to the surface and the tendency of the atoms in Ring 4, upon radial reorientation, to adopt an average lattice parameter closer to that of the core material. Upon relaxation, we find that, for the CdSe (CdTe) core systems, the bond length between a Cd atom in Ring 3 and a Te (Se) atom at the surface differs by less than 1% from the bulk Cd−Se (Cd−Te) bond length of 2.63 Å (2.83 Å) across all strains considered. The second is the increased sensitivity of the VBM in CdSe compared with the VBM of CdTe, as pointed out earlier in regards to the slab calculations. In particular, as the CdSe region is stretched away from equilibrium, the added axial strain increases the VBM to a greater extent than the reduced axial compression increases the VBM of the CdTe region.

To quantify how the VBM changes across the rings with strain, we define the VBO as the absolute difference in the VBM between the outermost and innermost rings. For the CdSe core system, the VBO varies with strain from approximately 0.45 to 0.55 eV when at the *c* lattice parameter of CdSe and CdTe, respectively. Conversely, the VBO for the CdTe core system decreases with increasing *c* from 0.35 eV when at the lattice parameter of CdSe to 0.11 eV when at the lattice value of CdTe. At the strain-minimized lattice parameters, the CdSe core nanowire displays a VBO of 0.51 eV, while the CdTe core shows a VBO of 0.20 eV.

For the case of the 2/2 structure, the optimal lattice positions were determined to be 7.48 Å for the CdSe core and 7.15 Å for the CdTe core. That these values lie closer to the equilibrium values for the shell component is a direct result of the shell region containing roughly 75% of the atoms. This has implications on the band gaps and VBO obtained from the RDOS, as seen in Figure 9. For the CdSe core structure (Figure 9a), the band gap of each ring again increases with decreasing lattice parameter, but because the optimal and equilibrium CdTe *c* values are so close, the VBM and CBM of the two differ only slightly. In the CdTe core structure (Figure 9b), the behavior of the band gap mirrors that seen in the 3/1 case, decreasing upon axial compression.

An analysis of the band edges in these cross sections shows that the VBO behaves in a similar manner to the 3/1 heterostructures. For the CdSe core nanowires, the VBO again increases with *c* value from 0.17 to 0.24 eV when compressed at the lattice parameter of CdSe and CdTe, respectively. The VBO of the CdTe core system decreases with increasing *c* value

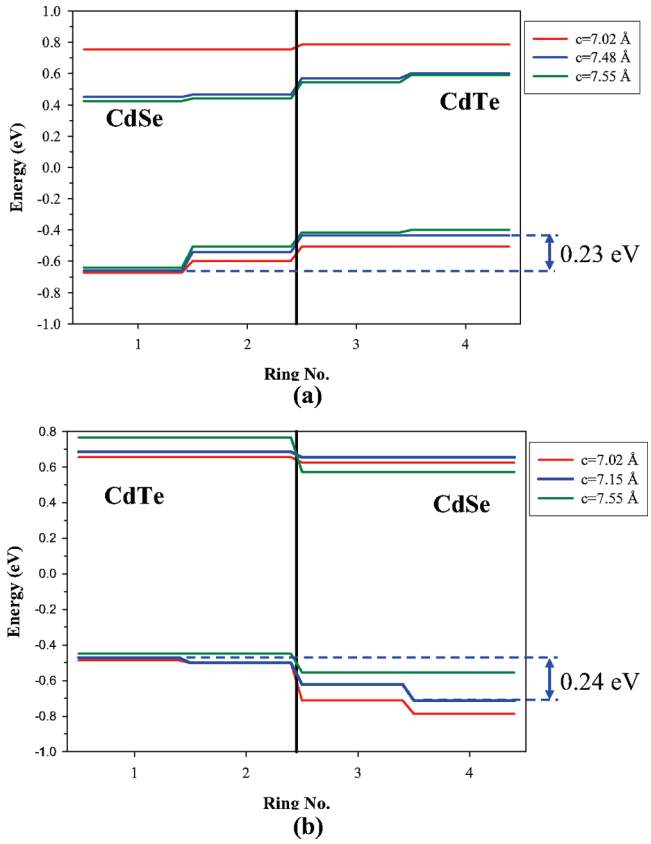

Figure 9. Band gap as a function of ring number for the different lattice constants considered, labeled according to the axial *c* value for the 2/2 (a) CdSe/CdTe and (b) CdTe/CdSe core/shell heterostructures. The zero point of energy was chosen to correspond to the Fermi energy. The solid vertical line indicates the location of the interface separating CdSe from CdTe. The VBO indicated on the plot corresponds to the optimal (strain-minimized) structure and is taken as the difference between the innermost and outermost VBM.

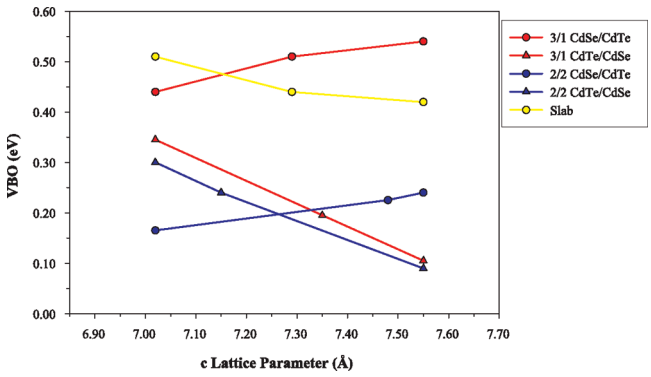

Figure 10. Valence band offset as a function of the axial *c* lattice parameter for the two-dimensional and one-dimensional heterostructures considered in this study.

from 0.30 eV to about 0.1 eV. The VBOs of the optimal structures in both the CdSe core and the CdTe core cases are quite similar and are on the order of 0.25 eV.

A summary of the effect of strain on the VBO for the different core/shell nanowires described above is presented in Table 2 as well as Figure 10. For comparison, the results of the heterostructure slab have also been plotted. Several interesting trends emerge. In all cases, there is approximately a linear relationship between axial strain and the VBO. In the CdTe core nanowires as well as the two-dimensional heterostructures, the VBO increases as the system is compressed. Conversely,

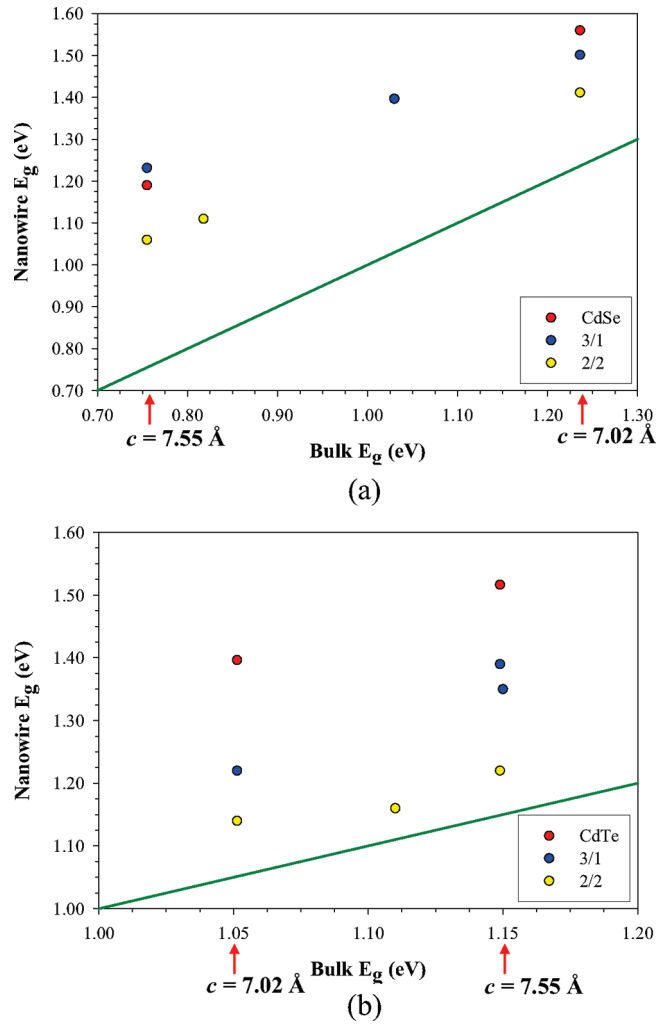

Figure 11. Band gap of the innermost (a) CdSe and (b) CdTe rings of nanowires as a function of the corresponding band gap of bulk held at the same *c* lattice value. The green line with a slope of 1 represents a perfect one-to-one agreement between the bulk and nanowire systems. The upward shift of all nanowire band-gap values with respect to the green line reflects the effect of quantum confinement.

in the CdSe core nanowires, the VBO increases with increasing *c*. To understand this opposite behavior, consider again Figures 8 and 9. In the CdSe core nanowires, stretching the system causes the difference between the VBM in Ring 1 and the interface ring to increase. However, the difference in the VBM energies between CdSe and CdTe on either side of the interface is roughly constant in these structures, regardless of the strain or number of CdTe rings in the shell. The opposite behavior is observed when CdTe is the core material. In particular, the difference in energies between the VBM in the innermost and the interface ring is, in general, quite small and insensitive to the *c* lattice parameter. Moreover, the difference in VBM energies on either side of the interface is no longer constant but decreases with increasing *c*. Regardless of the material in the core, it is the increased sensitivity of the VBM in CdSe to strain relative to the VBM of CdTe that accounts for a significant portion of the VBO.

Figure 11 summarizes the band gaps of the innermost (a) CdSe and (b) CdTe rings for each of the systems considered in this study, plotting them against the bulk band-gap values of the appropriate bulk system held at the identical *c* lattice parameter. For reference, the bulk band-gap values of CdSe and CdTe at an axial lattice value of 7.02 and 7.55 Å have been

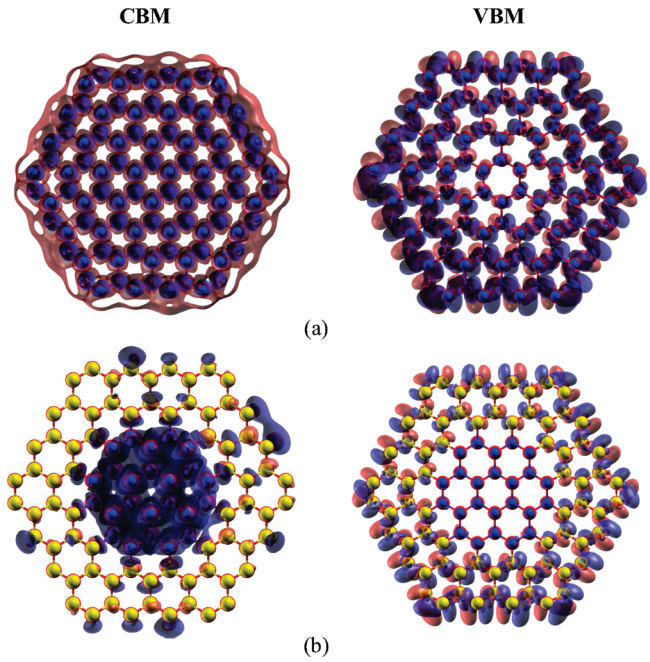

Figure 12. CBM and VBM wave function plots for (a) CdSe and (b) and 2/2 CdSe core nanowires, each lying at their strain-minimized lattice coordinates.

marked on each. At either *c* lattice parameter, the band gaps of the single-component nanowires are roughly 0.3−0.4 eV larger than the corresponding bulk values (represented by the straight line) due to quantum confinement. Consistent with bulk results, the band gap across the inner ring is larger when the nanowire is lying at its unstrained coordinates. Strain effects reduce the band gap of the CdSe nanowire by ≈0.4 eV, which is slightly less than the decrease observed when stretching the bulk to 7.55 Å, as shown in Table 2. Compressing CdTe to 7.02 Å reduces the band gap by only 0.1 eV in both the nanowire and the bulk.

As with the bulk and single-component systems examined earlier, the band gaps of the CdSe and CdTe core rings increase and decrease, respectively, with decreasing *c*. Although these band gaps are still larger than the bulk values, they are lower than their single-component analogues. Moreover, the band gaps of the 3/1 heterostructure are consistently larger than those of the 2/2 heterostructure over the range of strains considered. In general, the band gap of the optimal nanowire lies along a straight line connecting the band gaps of the nanowire compressed to 7.02 Å and stretched to 7.55 Å.

3. Electron−Hole Wave Function Overlap. To assess the impact of strain on the tendency for charge separation at the interface of the heterostructures, the wave functions corresponding to the CBM and VBM were plotted, under the assumption that an electron and hole would occupy these states upon dissociation of an exciton. Within each cross section, there was little visual difference in the plots when *c* was varied. Figure 12 shows our results for the single-component CdSe and 2/2 heterostructure, each lying at their strain-minimized coordinates. These results are qualitatively similar to those obtained for the other nanowires. Consistent with other II−VI studies,[18,46] the CBM states are shown to have an s-type character, while the VBM states have a strong p-type symmetry. In the single-component nanowires, these states are uniformly spread throughout the cross section. In the 2/2 topology, the impact of an interface on the location of the VBM and CBM wave functions is evident. The s orbitals of the CBM and the p orbitals of the VBM are highly localized in the CdSe core and the CdTe shell, respectively. This behavior is also seen in the 3/1, as well as in the CdTe core nanowires.

The physical separation of the VBM and CBM suggests that charge separation of an exciton into an electron and hole at the interface is feasible. To quantify this, the overlap of the VBM and CBM wave functions, $\psi_v(\mathbf{r})$ and $\psi_c(\mathbf{r})$ was computed using the following formula:

$$S = \int |\psi_v^*(\mathbf{r})||\psi_c(\mathbf{r})|\, d\mathbf{r} \quad (1)$$

The results of these calculations are presented in Table 2. The value of this integral lies between 0 and 1, with the former indicating complete separation and the latter complete overlap of the two wave functions. Every core/shell nanowire has an overlap lower than the values computed for the single-component nanowires, indicating a higher probability of charge separation in the former. Moreover, the choice of core material has little effect on the overlap. Straining the core/shell systems appears to provide a means of tailoring the overlap, as axial compression or stretching tends to slightly increase or decrease the overlaps relative to the strain-minimized values. Additionally, the overlap decreases with increasing shell thickness, indicating that, at sufficiently large core and shell thicknesses, the CBM and VBM wave functions ought to completely dissociate.

IV. Summary

We have presented a comprehensive ab initio study of the impact of uniaxial strain on the electronic properties of wurtzite CdSe and CdTe systems in bulk, thin-film, and nanowire geometries. Our results can be summarized as follows:

• Increasing the *c* lattice parameter of bulk CdSe results in a decrease in the band gap, as expected in sp^3-bonded covalent systems. Conversely, CdTe behaves anomalously upon compression, initially increasing upon compression, but goes through a maximum and decreasing upon further compression. At large compressions (greater than ≈7% from equilibrium), a transition from sp^3 to sp^2 hybridization is observed.

• Sufficiently far from the interface in the two-dimensional heterostructure slabs, the approximate bulk CdSe and CdTe band gaps are recovered. We also find that the valence band offset (VBO) decreases with increasing *c* lattice parameter.

• The behavior of single-component CdSe and CdTe nanowires when subjected to an axial strain is consistent with bulk calculations. Both CdSe and CdTe experienced a decrease in band gap when strained away from their equilibrium positions, although the absolute value of the band gap is larger than the corresponding bulk value due to quantum confinement.

• The impact of strain on the VBO in core/shell heterostructure nanowires was found to depend on the choice of core material. When CdSe is used as the core material, the VBO increases with increasing *c* lattice parameter, whereas when CdTe is used as the core material, the VBO decreases with increasing *c*.

• In single-component nanowires, there is a significant overlap between electron and hole states, whereas in the core/shell nanowires, the overlap is significantly low. Uniaxial strain along the nanowire axis does not appreciably change the overlap, although tension and compression slightly decrease and increase the overlap, respectively.

In conclusion, these results indicate that strain can be used to effectively tune the properties of core/shell nanowires for photovoltaic devices. Through the appropriate choices of

materials and strain, the potential exists to tailor *both* the band gap and the band offset, thereby achieving high conversion efficiencies and efficient charge separation simultaneously.

Acknowledgment. The authors would like to acknowledge financial support of this work through a grant from the National Science Foundation (NSF) and computational support through an NSF Teragrid Resource Allocation. Useful discussions with Dr. Leonardo Fonseca are also gratefully acknowledged.

References and Notes

(1) Lewis, N. S. *Science* **2007**, *315*, 798–801.
(2) Nozik, A. J. *Inorg. Chem.* **2005**, *44*, 6893–6899.
(3) Würfel, P. *Physics of Solar Cells*; Wiley-VCH: Darmstadt, Germany, 2005.
(4) Schaller, R. D.; Klimov, V. I. *Phys. Rev. Lett.* **2004**, *92*, 186601.
(5) Hepplestone, S. P.; Srivastava, G. P. *Nanotechnology* **2006**, *17*, 3288–3298.
(6) Beard, M. C.; Knutsen, K. P.; Yu, P.; Luther, J. M.; Song, O.; Metzger, W. K.; Ellingson, R. J.; Nozik, A. J. *Nano Lett.* **2007**, *7*, 2506–2512.
(7) Schleife, A.; Rödl, C.; Fuchs, F.; Furthmüller, J.; Bechstedt, F. *Appl. Phys. Lett.* **2007**, *91*, 241915.
(8) Milliron, D. J.; Hughes, S. M.; Cui, Y.; Manna, L.; Li, J.; Wang, L. W.; Alivisatos, A. P. *Nature* **2004**, *430*, 190–195.
(9) Schaller, R. D.; Agranovich, V. M.; Klimov, V. I. *Nat. Phys.* **2005**, *1*, 189–194.
(10) Kumar, S.; Jones, M.; Lo, S. S.; Scholes, G. D. *Small* **2007**, *3*, 1633–1639.
(11) Scholes, G. D. *ACS Nano* **2008**, *2*, 523–537.
(12) Franceschetti, A.; Wang, L. W.; Bester, G.; Zunger, A. *Nano Lett.* **2006**, *6*, 1069–1074.
(13) Piryatinski, A.; Ivanov, S. A.; Tretiak, S.; Klimov, V. I. *Nano Lett.* **2007**, *7*, 108–115.
(14) Kumar, S.; Nann, T. *Small* **2006**, *2*, 316–329.
(15) Reiss, P.; Protiére, M.; Li, L. *Small* **2009**, *5*, 154–168.
(16) Gur, I.; Fromer, N. A.; Geier, M. L.; Alivisatos, A. P. *Science* **2005**, *310*, 462–465.
(17) Law, M.; Greene, L. E.; Johnson, J. C.; Saykally, R.; Yang, P. *Nat. Mater.* **2005**, *4*, 455–459.
(18) Schrier, J.; Demchenko, D. O.; Wang, L. W. *Nano Lett.* **2007**, *7*, 2377–2382.
(19) Czaban, J. A.; Thompson, D. A.; LaPierre, R. R. *Nano Lett.* **2009**, *9*, 148–154.
(20) Tian, B.; Kempa, T. J.; Lieber, C. M. *Chem. Soc. Rev.* **2009**, *38*, 16–24.
(21) Beach, J. D.; McCandless, B. E. *MRS Bull.* **2007**, *32*, 225–229.
(22) Pilania, G.; Sadowski, T.; Ramprasad, R. *J. Phys. Chem C* **2009**, *113*, 1863–1871.
(23) Lauhon, L. J.; Gudiksen, M. S.; Wang, D.; Lieber, C. M. *Nature* **2002**, *420*, 57–61.
(24) Lu, W.; Xiang, J.; Timko, B. P.; Wu, Y.; Lieber, C. M. *Proc. Natl. Acad. Sci. U.S.A.* **2005**, *102*, 10046–10051.
(25) Ertekin, E.; Greany, P. A.; Chrzan, D. C.; Sands, T. D. *J. Appl. Phys.* **2005**, *97*, 114325.
(26) Nduwimana, A.; Musin, R. N.; Smith, A. M.; Wang, X. Q. *Nano Lett.* **2008**, *8*, 3341–3344.
(27) Swadener, J. G.; Picraus, S. T. *J. Appl. Phys.* **2009**, *105*, 044310.
(28) Wei, S. H.; Zunger, A. *Appl. Phys. Lett.* **1998**, *72*, 2011.
(29) Wei, S. H.; Zhang, S. B.; Zunger, A. *J. Appl. Phys.* **2000**, *87*, 1304–1311.
(30) Martin, R. *Electronic Structure: Basic Theory and Practical Methods*; Cambridge University Press: New York, 2004.
(31) Soler, J. M.; Artacho, E.; Gale, J. D.; Garcia, A.; Junquera, J.; Ordejon, P.; Sanchez-Portal, D. *J. Phys.: Condens. Matter* **2002**, *14*, 2745–2779.
(32) Perdew, J. P.; Zunger, A. *Phys. Rev. B* **1981**, *23*, 5048–5079.
(33) Vogel, D.; Krüger, P.; Pollmann, J. *Phys. Rev. B* **1995**, *52*, R14316–R14319.
(34) Yu, M.; Fernando, G. W.; Li, R.; Papadimitrakopoulos, F.; Shi, N.; Ramprasad, R. *Appl. Phys. Lett.* **2006**, *88*, 231910.
(35) Sadowski, T.; Ramprasad, R. *Phys. Rev. B* **2007**, *76*, 235310.
(36) Li, J.; Wang, L. W. *Phys. Rev. B* **2005**, *72*, 125325.
(37) Komsa, H. P.; Arola, E.; Larkins, E.; Rantala, T. T. *J. Phys.: Condens. Matter* **2008**, *20*, 315004.
(38) Troullier, N.; Martin, J. L. *Phys. Rev. B* **1991**, *43*, 1993–2006.
(39) Monkhorst, H. J.; Pack, J. D. *Phys. Rev. B* **1976**, *13*, 5188–5192.
(40) Zakharov, O.; Rubio, A.; Blase, X.; Cohen, M. L.; Louie, S. G. *Phys. Rev. B* **1994**, *50*, 10780.
(41) Hellwege, K. H., Madelung, O., Eds. *Landolt-Börnstein Numerical Data and Functional Relationships in Science and Technology*; Springer: New York, 1982.
(42) Neretina, S.; Hughes, R. A.; Britten, J. F.; Sochinskii, N. V.; Preston, J. S.; Mascher, P. *Nanotechnology* **2007**, *18*, 275301.
(43) Yadav, S. K.; Sadowski, T.; Ramprasad, R., unpublished.
(44) Shi, N.; Ramprasad, R. *IEEE Trans. Dielectr. Electr. Insul.* **2008**, *15*, 170–177.
(45) Van de Walle, C. G.; Martin, R. M. *Phys. Rev. B* **1986**, *34*, 5621–5634.
(46) Wei, S. H.; Zunger, A. *Phys. Rev. B* **1988**, *37*, 8958–8981.

JP907150D